Early detection of liver cancer based on bioluminescence tomography

Xibo Ma[1], Jie Tian[1]*, Chenghu Qin[1], Xin Yang[1], Bo Zhang[1], Zhenwen Xue[1], Xing Zhang[1], Dong Han[1], Di Dong[1], Xueyan Liu[1]

[1]Medical Imaging Processing Group, Institute of Automation, Chinese Academy of Sciences,

P. O. Box 2728, Beijing, 100190, China

[*]Corresponding author: tian@ieee.org; jietian@ia.ac.cn

As a new modality of molecular imaging, bioluminescence imaging (BLI) has been widely used in tumor detection and drug evaluation. However, BLI cannot present the depth of information for internal diseases such as a liver tumor *in situ* or a lung tumor *in*. In this paper, we described a bioluminescence tomography (BLT) method based on the bioluminescent intensity attenuation calibration and applied it to the early detection of liver cancer *in situ*. In comparison with BLT without calibration, this method could improve the reconstruction accuracy by more than 10%. In comparison with Micro-CT and other traditional imaging modalities, this method can detect a liver tumor at a very early stage and provide reliable location information.

OCIS codes: 170.3010，170.3880，170.6960，170.1420, 170.0170.

1. Introduction

Molecular imaging including bioluminescence imaging, fluorescent imaging, positron emission tomography (PET), single photon emission computed tomography (SPECT), and computed tomography (CT) can provide the imaging tools and instruments in process of tumor and drug development [1]. The aim of molecular imaging is to non-invasively depict the cellular and molecular processes of tumor progression qualitatively and quantitatively [2, 3]. Among molecular imaging modalities, optical molecular imaging including bioluminescence imaging and fluorescence imaging draw more and more attention due to high sensitivity and low cost. Combining innovative molecular biology and chemistry, optical molecular imaging has been used to image protein interactions [4-7], protease activity [8-10], protein degradation [11-13] and so on.

In recent years, bioluminescence imaging has been widely applied in tumor detection and anti-tumor drug evaluation [14]. However, bioluminescence imaging cannot present the accurate three-dimensional location of inner bioluminescent sources such as in the liver, bone or lungs. As a three-dimensional reconstruction method of bioluminescence, bioluminescence tomography (BLT) shows its advantage in determining the bioluminescence source distribution inside a phantom or a small animal. Meanwhile, many BLT reconstruction algorithms have been developed such as Tikhonov

regularization based on adaptive finite elements [15], a temperature-modulated bioluminescence tomography method [16], a Born-type approximation bioluminescence tomography method [17], a trust region method in the adaptive finite element framework [18], Bayesian Approach [19], Graph cuts [20] and others. These methods have been proven to be confident in reconstructing the source distribution in simulation and phantom experiments. Wang et al. described the *in vivo* mouse experiment with BLT [21]. Liu et al. performed the *in vivo* experiments, but the tumor model, which was created by injecting PC3-Luc prostate tumor cells with matrigel into the liver that was fixed at a point, could not reflect distinct tumor distribution and tumor characterization. Therefore, it did not belong to an actual tumor-bearing mouse model [22]. However, research on tumors *in situ* is very important, anywhere from tumor model building and mechanistic studies of tumor metastasis to anti-tumor drug evaluation. All of these studies need to provide reliable location information of tumors *in situ* for further research. The BLT method based on bioluminescent intensity decay calibration proposed in this paper can reconstruct the location information more accurately, which is reliable in tumor and anti-tumor drug studies.

Liver tumors are a common malignancy with a high mortality rate. Hepatocellular carcinoma LM3 (HCC-LM3) is a subtype of liver cancer found in Asia and has a high incidence [23, 24]. The study on its mechanism and relevant anti-tumor drugs is less than that in other liver tumors. The high metastasis component of HCC-LM3 makes it important for reconstructing the

three-dimensional location of the tumor for further study. In view of BLT's high sensitivity, early detection of liver cancer *in situ* is possible.

This paper is organized in the following sequence. In section 2, we present the report based on the experiment and data processing order. Firstly, we describe the cell culture conditions and animal model building methods. Secondly, the bioluminescent image acquisition method is introduced briefly in section 2.2. Thirdly, the bioluminescent intensity decay calibration experiments, Micro-CT data acquisition experiments and volume data reconstruction and the data preprocessing method are presented in section 2.3, 2.4 and 2.5 respectively. Finally, the reconstruction method is presented in section 2.5. In section 3, we compare two types of reconstruction results. The results show that the reconstruction based on the calibrated surface optical intensity can improve the reconstruction accuracy by more than 10%. Furthermore, compared with Micro-CT, BLT can detect the liver tumor at an early stage. This reconstruction result also coincides with the traditional biological method. In the final part of the paper, we give our comments and conclude the paper in section 4.

2. Experiments and methods

2.1 Cell culture and animal model

The firefly luciferase (fLuc) that transfected the HCC-LM3 human hepatocellular carcinoma cell line [23, 24] (HCC-LM3-fLuc) was kindly

provided by Prof. Jian Zhao of Shanghai Second Military Medical University. No significant difference between HCC-LM3 and HCC-LM3-fLuc cells was observed in terms of proliferation, tumorigenicity and migration.

HCC-LM3-fLuc human hepatocelluar carcinoma cells were grown in Dulbecco's Modified Eagle's Medium supplemented with 10% fetal bovine serum in a humidified incubator at 37^{o}C in a 5% CO_2 atmosphere. Male BALB/c nude mice (4~5 weeks of age) were purchased from the Department of Experimental Animals, Peking University Health Science Center. First, the HCC-LM3-fLuc initial tumor model was established by subcutaneous injection of 3×10^6 HCC-LM3-fLuc tumor cells into the right upper flanks of BALB/c nude mice. When the tumor volume reached about 50~100mm^3, the tumor was extracted and the tumor cells were cultivated in the cell culture bottle overnight. Finally, the cells were harvested and about 6×10^6 cells were injected into the mouse liver. Then, the mouse's incisions were closed, disinfected and the tumor-bearing mouse was returned and fed in the animal facility for the following experiments. Ten mouse models were built in total. All animal experiments were performed in accordance with the guidelines of the Institutional Animal Care and Use Committee at Peking University.

2.2 In vivo bioluminescent image acquisition

The *in vivo* bioluminescence imaging experiment was carried out on the seventh day after HCC-LM3-fLuc cells were inoculated in the liver. The mouse was fasted overnight prior to the experiment to prevent food from

interfering with the bioluminescence results. The mouse was affixed to the mouse bed after being injected with 200μl urethane, and then the mouse bed was assembled on the rotation stage (shown in Fig. 1, location 3). The rotation stage was set to rotate at 0^o, 90^o, 180^o and 270^o for taking four degree bioluminescent images. Four degree images were acquired respectively at the tenth, thirteenth, sixteenth and nineteenth minute after intraperitoneal injection of 200μl D-Luciferin (Biotium, Inc. CA, Fremont, USA). During imaging acquisition, parameters of CCD (Princeton Instruments PIXIS 1024BR, Roper scientific, Trenton, NJ) were set at exposure time = 2 min, f-number = 2.8, binning = 4, controller gain = 3, rate = 1 MHz, resolution = 16 bits, and read out = low noise. The experiments were carried out in a completely dark environment. In order to obtain absolute bioluminescent intensity, a 12-inch integrating sphere (USS-1200V-LL Low-Light Uniform Source, Labsphere Inc., USA) was used to calibrate the absolute intensity in physical units of the CCD output value. Bioluminescent intensity was quantified from the acquired image using Windows Molecular Imaging System (WinMI) software, which was developed based on the Medical Imaging ToolKit (MITK [25], medical image processing and analysis group, Institute of Automation, Chinese Academy of Sciences, Beijing, China; www.mitk.net). The four degree bioluminescent images are shown in Fig. 2 (a).

Figure 1

Figure 2

2.3 Bioluminescent intensity decay calibration

The liver tumor can be detected by capturing the bioluminescent photons that are generated by the oxidation of firefly luciferase and its specific substrate D-Luciferin in the presence of oxygen and ATP as a source of energy. The bioluminescent light intensity decreased along with the acquired four degree images, hence intensity decay calibration is necessary. In this experiment, seven anesthetized (2% isoflurane) HCC-LM3-fLuc tumor bearing mice were imaged in a light-tight chamber with light-emitting diodes (LED) located on its top to minimize any effects of light outside the chamber (ZKKS-MI-IV Imaging System, Guangzhou Zhongke Kaisheng Medical Technology Co. Ltd and molecular imaging research group, Institute of Automation, Chinese Academy of Sciences, Guangzhou & Beijing, China). After image acquisition, we calculated the average bioluminescent light intensity of seven mice at the same time after injecting D-Luciferin. The bioluminescent intensity at different times was plotted in Fig. 3, which shows the time-dependent-decay characterization of the bioluminescent source. The bioluminescent light intensity in the four images could be compensated based on the curve. The corresponding calibrated results are shown in Fig. 4.

Figure 3

Figure 4

2.4 Micro-CT imaging acquisition and reconstruction

The anatomical information was acquired by the Micro-CT system for the following bioluminescence distribution reconstruction. The Micro-CT system consists of a micro-focus X-ray source with a focal spot size of 30μm, a flat-panel X-ray detector with a 1120 × 1172 pixel photodiode array and 50μm pixel pitch (shown in Fig.1, location 2). During the imaging acquisition, the parameter of the Micro-CT was set as follows: voltage of X-ray tube was 60 kVp, the integration time of the detector was 0.467 sec, the size of each projection view was 1124×1134, and the pixel size of the detector was 0.1mm×0.1mm. In the second hour after injecting 200μl Fenestra VC through tail vein, 500 projection views were collected in 8.5 min. After acquiring the projection data, a GPU accelerated FDK method [26] was used to reconstruct the volume data (shown in Fig. 5); the type was 16 bits unsigned short point and the volume size was 512×512×256. The total time was 43.170 sec, which included reading the data from the disk and reconstructing the volume data.

Figure 5

2.5 Data preprocessing

Different organs were segmented and combined using the toolkit MITK for obtaining heterogeneous information from the mouse. A Gaussian filter was used to smooth the results, thereby interpolating small holes and gaps. Then, the bioluminescent intensity with calibration and without calibration was mapped on the mouse surface from the CT volume data according to the

registration point marked prior to the experiment (data shown in Fig. 2 (b) and Fig. 4 (b)). Since the emission peak wavelength of the bioluminescence was about 644nm, the optical parameters of different organs were computed at this wavelength based on previous literature reports [27] (as listed in table 1).

Table 1

2.6 Transformation of the diffusion equation

As the bioluminescence imaging experiment was carried out in a completely dark environment, the propagation of bioluminescent photons in the mouse tissue could be demonstrated by the steady-state diffusion equation and Robin boundary condition [28, 29].

$$-\nabla(D(\mathbf{x})\nabla\Phi(\mathbf{x})) + \mu_a(\mathbf{x})\Phi(\mathbf{x}) = S(\mathbf{x}) \quad (\mathbf{x} \in \Omega) \tag{1-1}$$

$$\Phi(\mathbf{x}) + 2A(\mathbf{x}; n, n')D(\mathbf{x})(v(\mathbf{x}) \cdot \nabla\Phi(\mathbf{x})) = 0 \quad (\mathbf{x} \in \partial\Omega) \tag{1-2}$$

Where Ω and $\partial\Omega$ are the domain and its boundary respectively; $\Phi(\mathbf{x})$ denotes the photon flux density [Watts/mm^2]; $S(\mathbf{x})$ is the source energy density [Watts/mm^3]; $\mu_a(\mathbf{x})$ is the absorption coefficient [mm^{-1}]; $D(x) = 1/(3(\mu_a(\mathbf{x}) + (1-g)\mu_s(\mathbf{x})))$ is the optical diffusion coefficient [mm]; $\mu_s(\mathbf{x})$ is the scattering coeffient [mm^{-1}]; and g is the anisotropy parameter. In this paper, we used six tissues to represent a heterogeneous mouse to reconstruct the tumor distribution, so the value of $\mu_a(\mathbf{x})$ $\mu_s(\mathbf{x})$ and g are different at different tissues (see table 1).Finally, v is the unit outer normal for

$\partial\Omega$. Based on the mismatch between the refractive indices n for Ω and n' for the external medium, $A(\mathbf{x};n,n')$ can be approximately represented as [28]:

$$A(\mathbf{x};n,n') = \frac{1+R(\mathbf{x};n,n')}{1-R(\mathbf{x};n,n')} \tag{2}$$

Usually, we do not consider the influence of $\mathbf{x}$, so that $R(\mathbf{x};n,n')$ is the function of n and n'.

When the mouse is suspended in the air, n' is close to 1.0 and $R(\mathbf{x};n,n')$ is approximated to be $-1.4399n^{-2}+0.7099n^{-1}+0.6681+0.0636n$ [28]. The measured quantity of the outgoing flux density $Q(x)$ on $\partial\Omega$ is:

$$Q(\mathbf{x}) = -D(\mathbf{x})(v\cdot\nabla\Phi(\mathbf{x})) = \frac{\Phi(\mathbf{x})}{2A(\mathbf{x};n,n')} \quad (\mathbf{x}\in\partial\Omega) \tag{3}$$

Based on the finite element theory [30], the equation can be finally transformed to

$$AS^p = \Phi^m \tag{4}$$

where Φ^m is the measurable boundary flux, and S^p is the unknown source density.

2.7 Bioluminescence decay calibration strategy and reconstruction method

In order to compensate the attenuation influence on Φ^m, we introduced the calibration strategy as follows:

According to the bioluminescent intensity data from the experiment in section 2.3, we calculated the average bioluminescent intensity of seven mice at every

time point and at maximum deviation $d_{\max}(t)$. Then, a cubic differentiable function $C(t)$ could be used to fit the bioluminescent intensity data.

When Φ^m was derived from the four angles at different times, we marked it as $\Phi_i^m \ (i = 1, 2, 3, 4)$.

After initial calibration $\Phi_i^m = \Phi^m + C(t_i)$, in order to evaluate the deviation of the calibration, the deviation function was defined as:

$$d(\mathbf{x}_j) = \frac{1}{N}\sum_{n=1}^{N}\left|\Phi^m(\mathbf{x}_j) - \Phi^m(\mathbf{x}_n)\right| \ \mathbf{x}_n \in \partial\Omega \bigcap \overline{B_r}(\mathbf{x}_j)$$

if $d(\mathbf{x}_j) > 0.5\Phi^m(\mathbf{x}_j)$, the value of $\Phi^m(\mathbf{x}_j)$ was assigned based on the equation

$$\Phi_C^m(\mathbf{x}_j) = \frac{1}{N}\sum_{n=1}^{N}\Phi^m(\mathbf{x}_n) \ \mathbf{x}_n \in \partial\Omega \bigcap \overline{B_r}(\mathbf{x}_j)$$

Then equation 4) becomes

$$AS^p = \Phi_C^m \tag{5}$$

In this paper, BLT is used to mathematically reconstruct the liver tumor distribution S^p according to the measured surface bioluminescence distribution Φ_C^m. Because BLT is an ill-posed inverse problem, we used Tikhonov regularization to compute the inner source distribution:

$$\min_{s_{\inf} \le S^p \le s_{\sup}} \{\left\| AS^p - \Phi_C^m \right\|_\Lambda + \lambda\eta(S^p)\} \tag{6}$$

where $s_{\inf}$ and $s_{\sup}$ are the lower and upper bounds of the source density; Λ is the weight matrix, so that $\left\|V\right\|_\Lambda = V^T\Lambda V$; and λ and η are the regularization

parameter and penalty function respectively. The convergence and stability of this method have been validated in both heterogeneous phantom models and homogeneous phantom models [15, 18-20].

3. Results

According to the reconstructed volume data from Micro-CT (shown in Fig. 5), the HCC-LM3-fLuc tumor-bearing mouse was segmented into 6 major organs including muscle, lungs, liver, spleen, heart and bone (shown in Fig. 7 (a)). Thus, the parameters $\mu_a(\mathbf{x})$ and $D(x)$ in equation (1-1， 1-2) are different in different tissues. Matrix A in corresponding matrix equation (5) is different in the homogeneous mouse. The reconstruction processor is run according to the parameters of different tissues (as listed in Table 1). The segmented CT volume data was discretized into 3604 points and 17031 tetrahedrons.

In order to induce the ill-posedness of reconstruction, we adopted a permissible source region strategy. According to the bioluminescence distribution on the surface after mapping (shown in Fig. 2 (b) and Fig. 4 (b)), the permissible source region (PS) was set to

$$PS = \{(x, y, z) \,|\, 12 < x < 24, 14 < y < 24, 28 < z < 40, (x, y, z) \in \Omega\}$$

The regularization parameter was set to 1.0×10^{-11} and the threshold was set to 0.5. The reconstruction time of the aforementioned method was 2465.2 sec. After reconstruction, we calculated the virtual volume ($V_{virtual}$) of the liver tumor located in the liver, and calculated the total volume (V_{total}) of the

reconstructed tetrahedrons as well. The volume of every tetrahedron was calculated by the absolute value of the following equation:

$$\frac{1}{6}\begin{vmatrix} x_1 & y_1 & z_1 & 1 \\ x_2 & y_2 & z_2 & 1 \\ x_3 & y_3 & z_3 & 1 \\ x_4 & y_4 & z_4 & 1 \end{vmatrix}$$

where (x_1, y_1, z_1), (x_2, y_2, z_2), (x_3, y_3, z_3), (x_4, y_4, z_4) are four vertices of the tetrahedron. The reconstruction accuracy was calculated by:

$$RA = \sum_{i=1}^{M} V^{i}_{virtual} \Big/ \sum_{j=1}^{N} V^{j}_{total}$$

where M is the number of reconstructed tetrahedrons which are located in the liver, and N is the total number of reconstructed tetrahedrons.

The reconstruction results based on heterogeneous mice are shown in Fig. 6. Meanwhile, we have reconstructed the bioluminescence distribution based on the calibrated bioluminescent intensity. The other parameters were set as same as the reconstruction without calibration. The reconstruction results based on the calibrated bioluminescent intensity are shown in Fig. 7.

From the Micro-CT volume data (shown in Fig. 5), we cannot discern a liver tumor from normal liver tissue because the tumor is at a very early stage, which is beyond the sensitivity of Micro-CT. However, both reconstruction figures (shown in Fig. 6 and Fig. 7) can show that the tumor occurred in the liver which was validated by the following pathology experiments. Through these experiments, we proved that the tumor had been successfully transplanted into the liver. After calibrating the bioluminescent intensity, 212

elements were reconstructed with a total volume of 203.97 mm^3, and 81.96% of that belong to the liver. Without calibration, 210 elements were reconstructed with a total volume of 219. 44mm^3, and the reconstruction accuracy was 69%. This result shows that calibration before reconstruction can improve accuracy by 12.96% (data listed in Table 2). The reconstructed bioluminescent light source beyond the liver may imply that the cells dissociated from the liver during inoculation, which needs to be verified in another study. This systematic detection and reconstruction method of the liver tumor *in situ* will provide reliable support for the study of liver tumor mechanisms and relevant pharmaceutical trials.

The above BLT experiments were carried out separately on the 0^{st} day, 3^{rd} day, and 7^{th} day after HCC-LM3-fLuc inoculation. The results showed that the bioluminescent intensity on the 7^{th} day was equal to the bioluminescent intensity on the 0^{st} day and two reconstruction results were almost equal to each other. On the 3^{rd} day, the bioluminescent intensity was too low and the information obtained from the boundary was inadequate for reconstruction. We thus concluded that the liver tumor could be reconstructed by BLT when the tumor cells increased to about 6×10^6 in the liver.

In addition, the BLT experiments were carried out on another two mice. The results showed that the reconstruction accuracy with calibration could be improved separately by 11.58% and 12.82% than reconstruction without calibration. All of the results from the three mice are shown in table 3.

Table 2

Table 3

Figure 6

Figure 7

4. Discussion and conclusions

Early detection of liver tumors is an emerging problem which is related to tumor diagnosis and anti-tumor drug efficacy evaluation. Bioluminescence imaging has been widely used in detecting subcutaneous tumors and evaluating the anti-tumor efficacy based on subcutaneous tumor bearing models. However, most *in situ* tumors are internal tumors such as liver tumors, lung tumors, and brain tumors, therefore bioluminescence imaging cannot generate the three-dimensional location of these tumors. BLTcan fill this gap for three-dimensional detection of *in situ* tumors.

BLT can be used to reconstruct the bioluminescence source distribution of liver tumors based on the surface light intensity information and anatomical information acquired. The bioluminescent source reconstruction results based on heterogeneous models proved to be efficient and accurate in both simulation and phantom experiments. Furthermore, through some *in vivo* experiments [21], the reconstructed results based on the heterogeneous mouse were also proven to be more accurate than the reconstructed results based on the homogeneous mouse. However, due to the ill-posedness and large computational cost of BLT in an *in vivo* application problem, *in vivo* experiments with meaningful biological models have not been done so far.

The BLT application in liver tumors introduced in this paper will promote this method's extensive application in biological and pharmaceutical areas. At the same time, in order to quickly obtain more accurate reconstruction results, greater effort needs to be made to improve the accuracy of reconstruction and shorten the time of the entire procedure.

In this paper, we introduced a BLT method based on bioluminescent intensity calibration and applied it in early detection of a liver tumor *in situ*. We systematically studied the reconstruction results based on the calibrated bioluminescent intensity and made comparisons with the reconstruction results without calibration. The results showed that this method could improve the reconstruction accuracy.

In the future, we will conduct *in vivo* experiments and reconstruction methods related to tumor metastasis. In addition, we will also study other influential factors to improve the reconstruction accuracy for widespread applications of BLT. Furthermore, because of the high sensitivity of bioluminescence and the low cost of the system, developing novel non-toxic probes for clinical application of BLT will be significant and meaningful to tumor treatment in the future.

Acknowledgments

This paper is supported by the National Basic Research Program of China (973 Program) under Grant Nos. 2006CB705700, 2011CB707700, the Knowledge Innovation Project of the Chinese Academy of Sciences under Grant No. KGCX2-YW-907, the National Natural Science Foundation of China under Grant Nos. 81027002, 81071205, the Hundred Talents Program of the Chinese Academy of Sciences, and the Science and Technology Key Project of Beijing Municipal Education Commission under Grant No. KZ200910005005.

References

1. J. Willmann, N. Bruggen, L. Dinkelborg, and S. Gambhir, "Molecular imaging in drug development," Nature **7**, 591-606 (2008).
2. R. Weissleder and V. Ntziachristos, "Shedding light onto live molecular targets," Nat Med. **9,** 123-128 (2003).
3. V. Ntziachristos, J. Ripoll, L. H. V. Wang, and R. Weissleder, "Looking and listening to light: the evolution of whole-body photonic imaging," Nature Biotechnol. **23,** 313-320 (2005).
4. R. Paulmurugan and S. Gambhir. "Monitoring protein-protein interactions using split synthetic renilla luciferase protein-fragment-assisted complementation," Anal Chem. **75**, 1584–1589 (2003).
5. K. Luker, M. Smith, G. Luker, S. Gammon, H. Piwnica-Worms, and D. Piwnica-Worms, "Kinetics of regulated protein-protein interactions revealed with firefly luciferase complementation imaging in cells and living animals," Proc Natl Acad Sci USA. **101**, 12288–12293 (2004).
6. R. Paulmurugan and S. Gambhir, "Novel fusion protein approach for efficient highthroughput screening of small molecule-mediating protein-protein interactions in cells and living animals," Cancer Res. **65**, 7413–7420 (2005).
7. I. Remy and S. Michnick, "A highly sensitive protein-protein interaction assay based on Gaussia luciferase," Nat Methods **3**, 969–971 (2006).
8. M. Funovics, R. Weissleder, and C. Tung "Protease sensors for bioimaging," Anal Bioanal Chem. **377**, 956–963 (2003).

9. J. Grimm, D. Kirsch, and D. Windsor, “Use of gene expression profiling to direct in vivo molecular imaging of lung cancer,” Proc Natl Acad Sci USA. **102**, 14404–14409 (2005).

10. T. Jiang, E. Olson, Q. Nguyen, M. Roy, P. Jennings, and R. Tsien. “Tumor imaging by means of proteolytic activation of cell-penetrating peptides,” Proc Natl Acad Sci USA. **101**, 17867–17872 (2004).

11. G. Luker, C. Pica, J. Song, K. Luker, and D. Piwnica-Worms, “Imaging 26S proteasome activity and inhibition in living mice,” Nat Med. **9**, 969–973 (2003).

12. G. Zhang, M. Safran, and W. Wei, “Bioluminescent imaging of Cdk2 inhibition in vivo,” Nat Med. **10**, 643–648 (2004).

13. M. Safran, W. Kim, and F. O’Connell, “Mouse model for noninvasive imaging of HIF prolyl hydroxylase activity: assessment of an oral agent that stimulates erythropoietin production,” Proc Natl Acad Sci USA. **103**, 105–110 (2006).

14. X. Ma, Z. Liu, J. Tian, and F. Wang, “ Dual-Modality Monitoring of Tumor Response to Cyclophosphamide Therapy in Mice with Bioluminescence Imaging and Small-Animal Positron Emission Tomography,” Mol Imaging (2010), in press.

15. Y. Lv, J. Tian, W. Cong, G. Wang, J. Luo, W. Yang, and H. Li, “A multilevel adaptive finite element algorithm for bioluminescence tomography,” Opt. Express **14** (18), 8211–8223 (2006).

16. G. Wang, H. Shen, and W. Cong, "Temperature-modulated bioluminescence tomography," Opt. Express **14**, 7852-7871 (2006).

17. W. Cong and K. Durairaj, "A Born-type approximation method for bioluminescence tomography," Med. Phys. **33**, 679-686 (2006).

18. B. Zhang, X. Yang, C. Qin, D. Liu, S. Zhu, J. Feng, and J. Tian, "A trust region method in adaptive finite element framework for bioluminescence tomography," Opt. Express **18**, 6477-6491 (2010).

19. J. Feng, K. Jia, C. Qin, G. Yan, S. Zhu, X. Zhang, J. Liu, and J. Tian, "Three-dimensional Bioluminescence Tomography based on Bayesian Approach," Opt. Express **17**, 16834–16848 (2009).

20. K. Liu, J. Tian, X. Yang, Y. Lu, C. Qin, S. Zhu, and X. Zhang, "A fast bioluminescent source localization method based on generalized graph cuts with mouse model validations," Opt. Express **18**, 3732–3745 (2010).

21. G. Wang, W. Cong, K. Durairaj, and M. Henry, "In vivo mouse studies with bioluminescence tomography", Opt. Express, **14** (17), 7801-7809 (2006).

22. J. Liu, Y. Wang, and J. Tian, "In vivo quantitative bioluminescence tomography using heterogenous and homogenyous mouse models," Opt. Express **57**, 2579-2582 (2010).

23. J. Zhao, L. Dong, and B. Lu, "Down-regulation of osteopontin suppresses growth and metastasis of hepatocellular carcinoma via induction of apoptosis," Gastroenterology **135**, 956–968 (2008).

24. J. Zhao, B. Lu, and H. Xu, "Thirty-kilodalton Tat-interacting protein suppresses tumor metastasis by inhibition of osteopontin transcription in human hepatocellular carcinoma," Hepatology **48**, 265–275 (2008).

25. J. Tian, J. Xue, and Y. Dai, "A novel software platform for medical image processing and analyzing," IEEE Trans Inf. Technol. Biomed. **12**, 800–812 (2008).

26. G. Yan, J. Tian, S. Zhu, Y. Dai, and C. Qin, "Fast cone beam ct image reconstruction using gpu hardware. J. X-Ray SCI Technol. **16**, 225-234 (2008).

27. G. Alexandrakis, F.Rannou, and A. Chatziioannou, "Tomographic bioluminescence imaging by use of a combined optical-PET (OPET) system: a computer simulation feasibility study," Phys. Med. Biol. **50**, 4225-4242 (2005).

28. M. Schweiger, S. R. Arridge, M. Hiraoka, and D. T. Delpy, "The finite element method for the propagation of light in scattering media; Boundary and source conditions," Med. Phys. **22**, 1779-1792 (1995).

29. W. Cong, G. Wang, D. Kumar, Y. Liu, M. Jiang, L. V. Wang, E. A. Hoffman, G. McLennan, P. B. McCray, J. Zabner, and A. Cong, "Practical reconstruction method for bioluminescence tomography," Opt. Express **13**, 6756-6771 (2005).

30. S. S. Rao, The finite element method in engineering (Butterworth-Heinemann, 1999).

Table 1. Optical parameters of different heterogeneous mouse tissues

Material	μ_a [mm^{-1}]	μ_s [mm^{-1}]	g
Muscle	0.010	4.000	0.900
Lungs	0.350	23.000	0.940
Heart	0.200	16.000	0.850
Bone	0.002	20.000	0.900
Liver	0.035	6.000	0.900
Spleen	0.5461	7.1525	0.900

Table 2. The two reconstruction results with calibration and without calibration

Reconstruction condition	Without calibration	With calibration
Number of Reconstructed Elements	210	212
Total volume (mm^3)	219.44	203.97
Reconstruction accuracy	69.00%	81.96%

Table 3. The reconstruction results from three mice with calibration and without calibration

Mouse	RA Without calibration	RA With calibration
Mouse1	81.96%	69.00%
Mouse2	84.15%	72.57%
Mouse3	82.16%	69.34%

RA: reconstruction accuracy

List of Figure Captions

Fig. 1. Our prototype BLT/Micro-CT dual modality imaging system. (1) CCD camera; (2) X-ray detector; (3) mouse bed; (4) X-ray tube; (5) anesthesia machine; (6) rotation stage.

Fig. 2. (a), Four view overlay images from bioluminescent images and corresponding photographs of the HCC-LM3-fLuc bearing nude mouse without calibration. 0^o, anterior-posterior; 90^o, left lateral; 180^o, posterior-anterior; 270^o, right lateral image. (b) Absolute irradiance distribution on the mouse surface after mapping from 2D bioluminescence data.

Fig. 3. Time-dependent bioluminescent intensity decay curve.

Fig. 4. (a), Four view overlay images from bioluminescent images and corresponding photographs of the HCC-LM3-fLuc bearing nude mouse after calibrating the bioluminescent intensity. 0^o, anterior-posterior; 90^o, left lateral; 180^o, posterior-anterior; 270^o, right lateral image. (b) Absolute irradiance distribution on the mouse surface after mapping from 2D bioluminescence data with intensity calibration.

Fig. 5. Micro-CT volume data of the HCC-LM3-fLuc bearing nude mouse.

(a), coronal image; (b), transect image; (c), sagittal image.

Fig. 6. Four subfigures which are the reconstructed bioluminescence distribution at different angles based on the heterogeneous mouse without calibrating the bioluminescent intensity. The dark blue color is the liver. Number 1-4 label the prominent differences between the two reconstruction results.

Fig. 7. Four subfigures which are the reconstructed bioluminescence distribution at different angles based on the heterogeneous mouse after calibrating the bioluminescent intensity. The dark blue color is the liver.

Fig.1

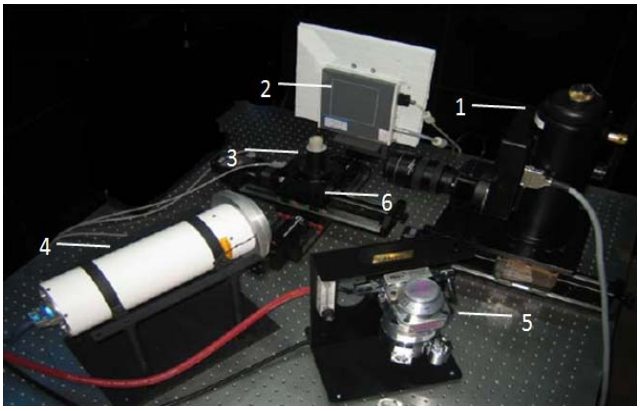

Fig.2

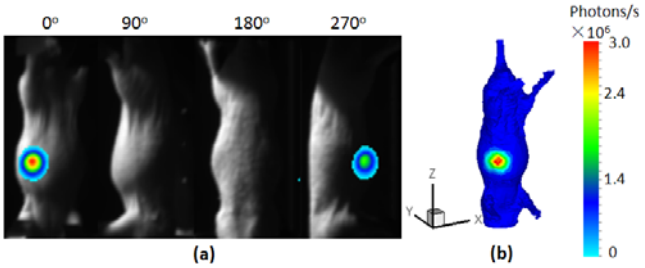

Fig.3

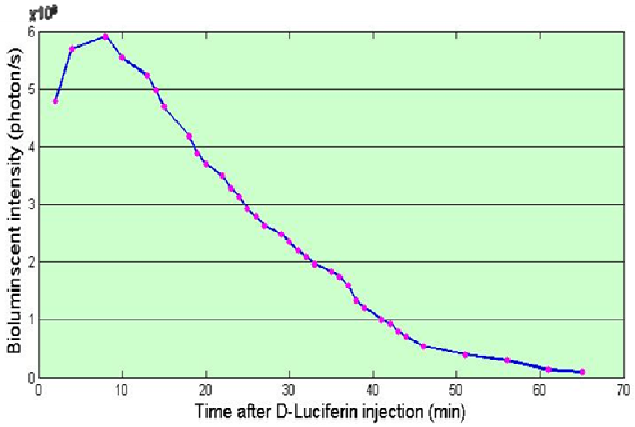
x10⁸
Bioluminescent intensity (photon/s)
Time after D-Luciferin injection (min)
0
1
2
3
4
5
6
0
10
20
30
40
50
60
70

Fig.4

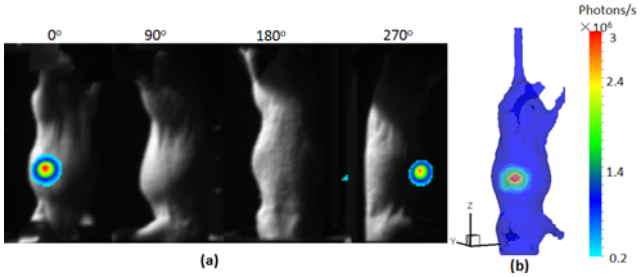

Fig.5

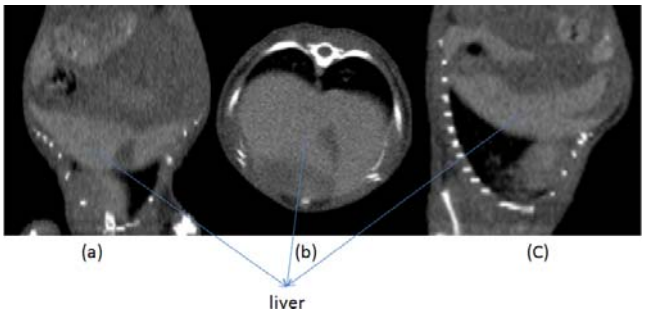

Fig.6

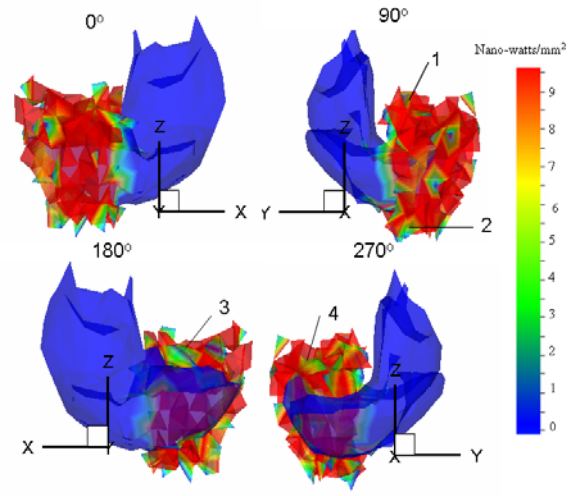

Fig.7